

111-37
207538
22 P

Measurements of the Influence of Integral Length Scale on Stagnation Region Heat Transfer

G. James Van Fossen
Lewis Research Center
Cleveland, Ohio

(NASA-TM-106503) MEASUREMENTS OF
THE INFLUENCE OF INTEGRAL LENGTH
SCALE ON STAGNATION REGION HEAT
TRANSFER (NASA) 22 p

N94-25183

and

Unclass

Chang Y. Ching
Syracuse University
Syracuse, New York

G3/34 0207538

Prepared for the
Fifth Symposium on Transport Phenomena and Dynamics of Rotating Machinery
sponsored by the Pacific Center of Thermal Fluids Engineering
Kaanapali, Hawaii, May 8-11, 1994



National Aeronautics and
Space Administration

Measurements of the Influence of Integral Length Scale on Stagnation Region Heat Transfer

G. James Van Fossen
National Aeronautics and Space Administration
Lewis Research Center
Cleveland, Ohio 44135

and

Chang Y. Ching
Syracuse University
Syracuse, New York 13210

ABSTRACT

The purpose of the present work was twofold: first, to determine if a length scale existed that would cause the greatest augmentation in stagnation region heat transfer for a given turbulence intensity and second, to develop a prediction tool for stagnation heat transfer in the presence of free stream turbulence. Toward this end, a model with a circular leading edge was fabricated with heat transfer gages in the stagnation region. The model was qualified in a low turbulence wind tunnel by comparing measurements with Frossling's solution for stagnation region heat transfer in a laminar free stream. Five turbulence generating grids were fabricated; four were square mesh, biplane grids made from square bars. Each had identical mesh to bar width ratio but different bar widths. The fifth grid was an array of fine parallel wires that were perpendicular to the axis of the cylindrical leading edge.

Turbulence intensity and integral length scale were measured as a function of distance from the grids. Stagnation region heat transfer was measured at various distances downstream of each grid. Data were taken at cylinder Reynolds numbers ranging from 42,000 to 193,000. Turbulence intensities were in the range 1.1 to 15.9 percent while the ratio of integral length scale to cylinder diameter ranged from 0.05 to 0.30.

Stagnation region heat transfer augmentation increased with decreasing length scale. An optimum scale was not found. A correlation was developed that fit heat transfer data for the square bar grids to within $\pm 4\%$. The data from the array of wires were not predicted by the correlation; augmentation was higher for this case indicating that the degree of isotropy in the turbulent flow field has a large effect on stagnation heat transfer. The data of other researchers are also compared with the correlation.

INTRODUCTION

Heat transfer to a stagnation region is important in many engineering applications; none, however, is more critical than in the gas turbine where combustor exit temperatures often exceed the melting point of superalloy turbine airfoil materials. In most cases the highest heat transfer rate on a turbine airfoil occurs in the stagnation region thus making it critical for the design of cooling schemes to obtain an accurate prediction in this region.

For a laminar free stream, the stagnation region can be modelled as a circular or elliptical cylinder in cross flow and the heat transfer can be found if the pressure distribution is known [1]. Free stream turbulence can augment stagnation region heat transfer; ratios of turbulent to laminar heat

transfer as high as 1.7 have been measured. In a gas turbine the stream of combustion products approaching an airfoil is not laminar; turbulence intensities of 11% have been measured at the exit of a combustor [2]; modern, high enthalpy rise combustors probably produce even higher levels.

Stagnation region heat transfer augmentation in the presence of free stream turbulence is believed to be caused by vorticity amplification (see [3] for a review). Free stream turbulence can be viewed as a continuum of tangled, vortical filaments; those filaments with components normal to the stagnation line and normal to the free stream flow are convected into the stagnation region where they are stretched and tilted by the divergence of streamlines and acceleration around the bluff body. This stretching causes the vorticity to be intensified through conservation of angular momentum. It has been shown both experimentally and numerically [4,5,6] that vorticity in the stagnation region causes heat transfer to be increased while the boundary layer remains laminar.

Turbulent eddies that are very large relative to the size of the bluff body are not stretched and thus act only as mean flow variations while eddies that are very small are destroyed by viscous dissipation before they can interact with the boundary layer. This leads to the hypothesis that somewhere between these two extremes there must be an optimum eddy size that causes the highest heat transfer augmentation. Two goals of this research were to determine this optimum eddy size and to develop a more accurate correlation that could be used by designers to predict heat transfer.

It has been known for many years that free stream turbulence can augment stagnation region heat transfer [7,8]; however, results of experiments are inconsistent and attempts to correlate heat transfer augmentation as a function of turbulence intensity and Reynolds number while ignoring the length scale [9,10,11,12,13] have not been entirely successful. Any resulting correlations usually predict the author's data but not data from other researchers.

Lowery and Vachon [14] measured lateral length scale in their study of the effect of grid generated turbulence on stagnation region heat transfer but they did not have a sufficient variety of grids to deduce an effect of scale. Their resulting correlation has been used as a standard against which subsequent data sets have been compared, sometimes with large discrepancies; see for example [15].

There have been several attempts to isolate the effect of turbulence length scale; Yardi and Sukhatme [16] used four different grids to generate a range of length scales. The four grids were all of different geometry; i.e. two were screens and two were biplane grids, all had different rod spacing to rod diameter ratios. They showed a trend of increasing heat transfer with decreasing length scale; however, there is so much scatter in the data that their claim of ten boundary layer thicknesses for an optimum length scale is questionable.

Dyban et al [17] used perforated plates as well as a fully developed turbulent pipe flow to investigate the effect of intensity and scale on stagnation region heat transfer. Their results showed increasing augmentation with decreasing scale but they did not attempt to correlate the data based on this finding.

More recently, Ames [18] used simulated combustor segments to generate turbulence and measure its effect on heat transfer to a flat plate and a stagnation region. Ames concentrated on relatively large scale turbulence where the length scale to leading edge diameter ratio was greater than 1.0. He used the rapid distortion theory of Hunt [19] and the measurements of Hunt and Graham [20] near a plane surface to develop a model for the spectrum of turbulence near stagnation. He integrated his model spectrum to estimate the eddy viscosity in the stagnation region. The viscosity was then used in a phenomenological model after Smith and Kuethe [11] to develop a new correlating

parameter involving Reynolds number, turbulence intensity, and what Ames calls an energy scale (the average size of the energy containing eddies). Ames used three different diameter cylinders to investigate stagnation region heat transfer; his data were well correlated using his new parameter. The data of several other researchers [14,17] were also correlated by his parameter but with more scatter.

For the present work, a model with a circular leading edge was fabricated with heat transfer gages in the stagnation region. The model was qualified in a low turbulence flow by comparing measurements with Frossling's solution for stagnation region heat transfer. Five turbulence generating grids were fabricated; four were square mesh, biplane grids made from square bars with different bar widths. Each of the four had identical mesh to bar width ratio. The fifth grid was an array of fine parallel wires that were perpendicular to the axis of the cylindrical leading edge.

Turbulence intensity and integral length scale were measured as a function of distance from the grids. Stagnation region heat transfer was measured with each grid at various distances upstream of the model. Data were taken at cylinder Reynolds numbers ranging from 42,000 to 193,000. Turbulence intensities were in the range 1.1 to 15.9 percent while the ratio of integral length scale to cylinder diameter ranged from 0.05 to 0.3.

Measurements of length scale and intensity are presented as well as the stagnation region heat transfer results. A correlation involving the turbulence parameters and Reynolds number is presented that fits the heat transfer data for the square bar grids to within $\pm 4\%$. The data of other researchers will also be compared with the correlation. Heat transfer data from the array of parallel wires will also be discussed. Finally, a method for determining the heat transfer distribution downstream of the stagnation point will be presented.

NOMENCLATURE

A	surface area of gage, m^2
A_{Fr}	constant in equation (11)
a	constant in fit of intensity, eqn. (9)
B	tunnel blockage
b	turbulence grid bar width, cm
C	constant in equation (11)
C_{hw}	constant in King's law, eqn. (7)
C_τ	parameter in equation (1)
d	diameter of leading edge ($=2R$), cm
E	mean hot wire voltage, V
e_{rms}	rms of linearized bridge voltage, V
$Fr(s/R)$	Frossling number
I	constant in eqn. (10)
k	thermal conductivity of air, W/mK
M	turbulence grid mesh spacing, cm
m	exponent in fit of intensity, eqn. (9)
n	exponent in King's law, eqn. (7)
p	exponent in fit of length scale, Tbl. II
Pr	Prandtl number
q	heat flow, W
R	leading edge radius, cm
Re	Reynolds number

$R(\tau)$	autocorrelation function of velocity
r	recovery factor
s	surface distance from stagnation, cm
T	temperature, $^{\circ}C$
Tu	turbulence intensity, %
U	mean velocity, m/s
u'	streamwise rms velocity, m/s
v'	spanwise rms velocity, m/s
x	streamwise distance, cm

Greek symbols

β	exponent in equation (11)
Λ	integral length scale of turbulence, cm
ξ	exponent in equation (11)
ρ	air density, Kgm/m^3
τ	time shift, s

Subscripts

0	evaluated at zero flow	<i>rad</i>	radiation
<i>avg</i>	averaged	<i>st</i>	static
<i>b</i>	bar width	<i>t</i>	total
<i>d</i>	leading edge diameter	<i>w</i>	wall
<i>EI</i>	electrical heating	<i>x</i>	streamwise
<i>gap</i>	epoxy filled gap between gages	<i>r</i>	recovery
<i>orf</i>	measured with orifice	∞	free stream conditions

TEST FACILITY & INSTRUMENTATION

Wind Tunnel

The experiments were carried out in the wind tunnel shown in figure 1, which is described in detail in [5]. Air flow drawn from the test cell passes through a flow conditioning section and a 4.85:1 contraction before entering the 15.2 cm wide by 68.6 cm high test section. The maximum velocity attainable was about 46 m/sec. Clear tunnel turbulence levels were less than 0.5 percent for all flow rates. After leaving the test section, the flow passed through a transition section into a 10-inch pipe in which a flow measuring orifice plate was located. Air then passed through a butterfly valve which was used to control the tunnel flow rate and then to the Laboratory exhaust system. The readings from four exposed-ball Chromel-Constantan thermocouples located around the perimeter of the inlet were averaged to yield the stagnation temperature. An actuator system with four degrees of freedom was used to position a hot wire probe at any desired measurement location within the rectangle shown on figure 1.

Turbulence Grids

Turbulence generating grids were installed at any one of several axial locations upstream of the model. For the present tests, five turbulence generating grids were used. Four were square bar, square mesh, biplane grids. The fifth grid consisted of an array of parallel wires oriented perpendicular to the streamwise and spanwise directions. Grid parameters are defined in figure 2 and dimensions of the grids are given in Table I. Henceforth grids will be referred to by the number given in the table. Grids G1 to G4 were fabricated keeping the ratio of mesh spacing to bar width constant at 4.5 yielding an open area of 60.5 percent. By having similar grids of different bar size, different length scales could be produced at fixed intensity by varying the distance from the grid.

Heat Transfer Model

The heat transfer model used in this study was a 6.60 cm thick flat plate that was 15.2 cm wide; the leading edge of the plate was a semi-circular cylinder. The flat plate extended 26.4 cm downstream from the tangent point to the cylinder and a 6.2° wedge then extended downstream and ended in a cylindrical trailing edge 0.635 cm in diameter. A photograph of the heat transfer model is shown in figure 3. Nineteen heat flux gages were embedded symmetrically around the stagnation line at 8.7° intervals so as to obtain heat transfer coefficients up to $\pm 78^\circ$ on either side of the stagnation line. Each heat flux gage consisted of an aluminum strip 6.60 cm long by 0.476 cm wide and 0.32 cm deep. A Kapton® encapsulated, foil, electric heater was fastened to the back of each aluminum strip with pressure-sensitive adhesive. Gage temperature was measured by a Chromel-Alumel thermocouple embedded in a groove in each aluminum strip. A guard heater behind the heat flux gages prevented heat conduction to the interior of the model. The average gap between the aluminum strips was 0.025 cm and was filled with epoxy. The aluminum strips were maintained at a uniform constant temperature by a specially designed control circuit, (see [21] for details). Steady state, spanwise-averaged heat transfer coefficients were calculated for each aluminum strip based on the

power supplied to the strip and the wall-to-fluid temperature difference.

Instrumentation and Data Acquisition

Turbulence measurements were obtained using a two channel, constant temperature, linearized, hot wire anemometer system. Turbulence intensities, and autocorrelations were measured using a standard, 5 μm , single, hot-wire oriented perpendicular to the flow direction. A cross-flow type X-wire probe was used for the two component measurements. The hot-wire signals were linearized with analog linearizers. For addition and subtraction of the signals from the X-wire, a signal conditioner was used. A programmable digital multimeter was used to calculate the root mean square (rms) velocity from the wires using 100-averages for each reading. Mean voltages were read on an integrating digital voltmeter with an adjustable time constant.

A dual channel spectrum analyzer was used to obtain autocorrelation data. The analyzer featured a 12-bit analog to digital conversion rate of 2.56 times the selected frequency and an anti-aliasing filter with a rolloff of 120 dB/octave. The selectable frequency range was from 10 Hz to 100 kHz. A personal computer was interfaced to the spectrum analyzer for data storage and processing.

Steady-state operating conditions (temperature, pressures, voltage and current to gages, etc.) were recorded on the Laboratory data acquisition system called ESCORT [22]. For every heat transfer data point, twenty readings of each data channel were recorded. These twenty readings were averaged to give a single value for each channel. To eliminate any offset between data channels caused by the solid state multiplexers, a reading was obtained by shorting all the inputs to ESCORT and subtracting this "zero" from each subsequent reading.

EXPERIMENTAL PROCEDURE

Hot wire calibration

The hot-wires used for the turbulence measurements were calibrated in an open air jet at nearly the same temperature as the wind tunnel flow. Velocity calibrations were carried out using a two point, iteration method in conjunction with the signal linearizers [23]. The frequency response of the hot-wire anemometer system was estimated to be around 30 kHz using the standard square wave test.

For the two component velocity measurements, the correction factor in Champagne's equation [24] which accounted for the cooling due to the tangential velocity component along the wire was determined experimentally by varying the angle between the X-wire bisector and the jet between 35 and 55° at jet velocities of 23 and 46 m/sec. A least squares curve fit of Champagne's equation was then used to find the correction factor. Complete details of the hot wire calibration procedure are given in [25].

Heat Flux Measurements

For the heat transfer measurements, all 19 heat flux gages were heated to temperatures of either 46 or 54°C; the average recovery temperature of the air was about 27°C giving wall to air temperature ratios of approximately 1.06 or 1.1. All of the heat flux gages were maintained at the same temperature within $\pm 0.2^\circ\text{C}$. Heat flux measurement were carried out with each grid in at least 7 axial locations from the stagnation line of the leading edge. For each grid position, tests were performed at 5 Reynolds numbers ranging from 42,000 to 193,000.

DATA REDUCTION AND UNCERTAINTY ANALYSIS

Turbulence Intensity

Turbulence intensities were calculated from the single hot-wire and the X-wire. The local turbulence

intensity for the single wire was calculated as the ratio of the rms to mean linearized, bridge voltage. Two component turbulence intensities were calculated from the linearized signals of the X-wire using the method of Champagne [24].

Integral Length Scale

The integral length scale describes the average eddy size associated with the turbulence. There are at least three practical ways to obtain the integral-length scale (see [25]); however, the availability of a spectrum analyzer that could compute the autocorrelation and average any number of them together made this method the natural choice. With this method, Taylor's hypothesis that time and streamwise distance are related by the mean velocity is invoked. A single point autocorrelation is thus equivalent to a two point space correlation separated by streamwise distance. The area under the normalized autocorrelation function gives a time scale for the average eddy which when multiplied by the mean velocity yields the longitudinal integral length scale, Λ_x .

The autocorrelation method suffers from a problem with low frequency noise, i.e. low frequency noise keeps the autocorrelation from approaching zero in a consistent manner. Many investigators have used the first zero crossing as the upper limit of integration [18,26,27]. The dashed lines on figure 4 are a typical pair of autocorrelations taken behind our grid G1; examination of this figure makes it clear that integrating until the first zero crossing will give very different results for the length scale.

To eliminate the low frequency noise problem, it was decided to use a least squares fit of the autocorrelation by the exponential function, i.e.

$$R(\tau) = e^{-C_\tau \tau} \quad (1)$$

Data between $0.33 \leq R(\tau) \leq 1.0$ were used for the curve fit; the resulting fit is also seen on figure 4. The exponential function does not reproduce the autocorrelation for very small values of τ but the fit is satisfactory over the main range of interest and the problem of determining the upper limit of integration is solved. Integrating between 0 and ∞ and multiplying by the mean velocity, the longitudinal length scale then becomes,

$$\Lambda_x = \frac{U}{C_\tau} \quad (2)$$

If the hot wire is long compared to the length scale of the flow, errors in intensity and scale can result due to averaging of flow variations over the wire length. Correction for the hot wire length was not made for the present tests; the smallest integral scale measured was 2.6 times the active length of the hot wire.

Heat Transfer

Power from the electric heaters is removed from the aluminum strips by convection to the air, radiation to the surroundings, and conduction to the epoxy gap between the gages where it is convected to the air. An energy balance was solved for the Frossling number for each gage

$$Fr(S/R) = \frac{(q_{EI} - q_{rad} - q_{gap}) d}{A (T_w - T_r) k \sqrt{Re_d}} \quad (3)$$

where q_{EI} is the heat added by the heater (voltage x current), q_{rad} is the heat lost by radiation, and q_{gap} is the heat conducted away to the epoxy gap and the unguarded ends of the strips. An estimate of

the gap loss can be obtained from an exact solution for two-dimensional heat conduction in a rectangle half the epoxy gap width wide and the aluminum gage depth deep. Two adjacent sides are assumed insulated, one side held at the constant temperature of the aluminum strip and the final side convecting to the air at a known temperature. Details of this analysis are given in [21]. Corrections for radiation heat losses were also made assuming gray body radiation to black surroundings and an emissivity of 0.05 for the aluminum gage. Heat lost through the sides of the strips was on the order of 10 percent of the total heat flow, while the radiation heat losses were on the order of 0.2 percent. A is the exposed heat transfer gage surface area, T_w is the gage temperature, and T_r is the recovery temperature at the gage location calculated from

$$T_r = T_{st,\infty} + r (T_t - T_{st,\infty}) \quad (4)$$

$T_{st,\infty}$ is the static temperature upstream of the model. The recovery factor, r , was calculated as

$$r = 1 - \left(\frac{\rho U(s)}{(\rho U)_\infty} \right)^2 (1 - \sqrt{Pr}) \quad (5)$$

the mass flow ratio, $\rho U(s)/(\rho U)_\infty$ was found from a numerical solution of flow over the plate that included the tunnel walls [28].

The thermal conductivity and viscosity were evaluated at the free stream total temperature from equations given in [29]. Total temperature was used to evaluate the thermal properties because in [28], a numerical study showed that if the thermal properties were based on a reference temperature that involved the wall temperature, reversing the direction of heat flux (cooling the wall) caused an undesirable change in the Frossling number.

The Reynolds number, Re_δ , was based on the diameter of the leading edge and the mass-velocity averaged between the flow area with maximum model blockage and the unblocked flow area, i.e.

$$(\rho U)_{avg} = (\rho U)_{orf} \frac{(2-B)}{2(1-B)} = 1.053 (\rho U)_{orf} \quad (6)$$

where the blockage, B , is the ratio of leading edge diameter to tunnel height ($B=.096$).

Uncertainty Analysis

Twenty samples were obtained for each steady-state measurement and averaged to minimize random errors. Standard deviations were also obtained from the twenty samples and used as an estimate of random error. Estimates of the accuracy of each measuring instrument were then made, added to the random component, and combined by the method of Kline & McClintock [30]. Results of the uncertainty analysis indicated an average uncertainty (95% confidence) of $\pm 6.6\%$ for the Frossling number. The level of uncertainty introduced by the corrections made for the conduction heat losses from the sides and unguarded ends of the aluminum strips accounted for about 44 percent of the total uncertainty; percentages attributed to other variables were: recovery temperature - 20, gage temperature - 11, heater voltage - 8, heater current - 8, flow rate - 7, and thermocouple reference temperature - 2.

Error in turbulence intensity was estimated by assuming that the linearizer approximates King's law; i.e. the velocity could be expressed in terms of bridge voltage as

$$U = \left(\frac{E^2 - E_0^2}{C_{hw}} \right)^n \quad (7)$$

where E is the bridge output voltage, E_0 is the voltage at zero velocity, and n and C_{hw} are constants. Differentiating this expression and dividing by the velocity, one obtains an expression for turbulence intensity

$$Tu = \frac{dU}{U} = \frac{u'}{U} = \frac{2nEe_{rms}}{E^2 - E_0^2} \quad (8)$$

where dU is taken as the rms of the fluctuating component of velocity and dE has been replaced by the rms of the fluctuating component of bridge voltage, e_{rms} . The exponent, n , was assumed to be near 2.0 with an error of $\pm 10\%$. The method of error estimation described above was then applied to this expression; typical uncertainties estimated for the turbulence intensity measurements were on the order of $\pm 15\%$. Uncertainties of the turbulence length scale were assumed to be the same order as the turbulence intensity.

RESULTS AND DISCUSSION

Turbulence

Intensity. Variation of turbulence intensity without the model in the test section is shown versus dimensionless distance downstream of each grid in figure 5. All five grids were run at velocities of 11, 23, and 46 m/sec, the decay of the intensity is in qualitative agreement with the correlation of Baines and Peterson [31] which is also shown on the figure for reference. Each grid and Reynolds number had slightly different characteristics so intensity data for each case were fit with a power law of the form

$$Tu = a \left(\frac{x}{b} \right)^m \quad (9)$$

Coefficients for each of the fits appear in Table II and the curve for each case is shown on figure 5. Several spanwise traverses were made downstream of the grids; typically, the variation of turbulence intensity was around 5%.

Length scale. Figure 6 shows the variation of the integral length scale in the streamwise direction behind grids G1-G5. Increase in the integral length scale with distance from the grid is apparent in all cases. This is expected, since the smaller eddies dissipate faster than the larger eddies. Also shown on the figure is a correlation due to Roach [32]. Roach developed a theory to correlate the variation of micro-scale with distance from the grid. He states that it is not possible to develop a theory for the variation of integral scale with distance. He therefore assumed that the integral scale should follow the decay of micro-scale in the downstream direction but removed the Reynolds number dependence. His correlation has the form

$$\frac{\Lambda_x}{b} = I \left(\frac{x}{b} \right)^{0.5} \quad (10)$$

He determined from his data that $I=0.2$. The present data for the square bar, square mesh grids tend to be independent of Reynolds number and follow the square root of distance dependence as in Roach's correlation but the constant is larger. The data for the wire array do not follow the same square root of distance dependence and are dependent on Reynolds number. Therefore, data for the wire array for each Reynolds number was fit with a power law curve. The resulting constants for the curve fits for the length scale data for all the grids are given in Table II. Curve fits of the integral scale versus distance from the grid are compared to the data in figure 6. These curvefits were used to determine the value of length scale when evaluating the heat transfer dependence.

Isotropy. Figure 7 shows u'/v' versus x/b for grids G3 through G5; the ratio u'/v' is a measure of isotropy for the turbulence, a value of 1.0 would indicate isotropic flow in the plane of the stagnation stream sheet. Turbulence for the square-bar, square-mesh grids (G3 and G4) seems to be nearly isotropic while that for grid G5 shows highly non-isotropic behavior with u'/v' values depending on Reynolds number. The X-wire results for the streamwise turbulence component are in close agreement with those obtained using the single hot-wire. For example, values of the turbulence intensity with grid G3 calculated from the single hot-wire and the X-wire are within 8 percent of each other at all Reynolds numbers.

Heat Transfer

Verification. Heat transfer results in the leading edge region with no turbulence grid in the tunnel are shown in figure 8. Measured freestream turbulence intensity in this case was less than 0.5 percent. The ordinate for the heat transfer plots is the Frossling number plotted against surface distance from stagnation made dimensionless by the leading edge radius. Results are presented for four levels of Reynolds number and two levels of gage temperature; in all cases the data agree to within the estimated experimental error with the solution of Frossling [1] and a 2-dimensional numerical solution from the PARC code [28] thus confirming the accuracy of the experimental technique.

Stagnation region augmentation. Figure 9 shows the Frossling number at stagnation plotted against the correlating parameter, $TuRe_d^{1/2}$, developed by Smith and Kuethe [11]. Turbulence intensity and length scale correspond to those measured in the wind tunnel downstream of the grid at the axial location of the stagnation line of the cylinder without the model present and were calculated from the correlations in Table II. By moving a grid closer to the cylinder, turbulence intensity is increased while the length scale is decreased. The range of longitudinal length scale to leading edge diameter ratio varied from 0.05 to 0.30. The range of turbulence intensity varied from 1.1 to 15.9%. The range of length scale for each grid is indicated on the legend in the figure. Also shown on the figure is the correlation developed by Lowery and Vachon [14]. The Lowery and Vachon correlation predicts the heat transfer data only in a narrow range of scales and as the parameter $TuRe_d^{1/2}$ increases beyond about 40, the correlation turns downward instead of continuing up as the data indicate. It is notable that there is no optimum length scale in the range tested here; rather, the heat transfer augmentation continues to increase as scale decreases.

The stagnation heat transfer data for the square bar grids was fit with a function of the form

$$Fr(0) = A_{Fr} \sqrt{Tu Re_d^\xi \left(\frac{\Lambda_x}{d}\right)^\beta} + C \quad (11)$$

The constant, C , was set at the zero turbulence Frossling number of 0.939 calculated by the PARC-2D code, the constants A_{Fr} , ξ , and β were determined from a least square fit of the data. The curve fit and the data are compared on figure 10; the function correlates the data to within $\pm 4\%$ as shown by the bands drawn on either side of the correlation.

Recall, that the turbulence for grids G1 - G4 was shown to be isotropic; that for grid G5 (the array of parallel wires) was not. The stagnation heat transfer results for grid G5 are compared to the stagnation region heat transfer correlation in figure 11. It is obvious from this figure that anisotropic turbulence with the majority of its vorticity oriented normal to the axis of the leading edge causes increased augmentation over isotropic turbulence.

As discussed in the INTRODUCTION, Ames [18] developed a correlation for stagnation heat transfer data that involved a scale he called an energy-scale. An attempt was made to correlate our data using his parameter, however, results were not satisfactory.

Figure 12 is a comparison of the stagnation heat transfer data of other authors with the present correlation. For cases where the authors did not measure length scale, it was estimated using the correlations given in Table II. The data of Zapp [9] and Ames [18] fall well above of the $\pm 8\%$ band shown about the correlation. The turbulence generator of Ames was a simulated combustor segment and produced anisotropic turbulence. The turbulence generators of Zapp were not conventional grids; they consisted of 0.5" dowels (orientation not given) and "two screens next to each other". Not enough information is given about the generators to speculate on the cause of the discrepancy. The data of the other authors are in good agreement with the present correlation.

Distribution of heat transfer around leading edge. Figure 13 is a plot of the Frossling number normalized by the stagnation value versus dimensionless surface distance from the stagnation point. The symbols represent the average of the present data for all grids, Reynolds numbers, and grid positions. The dotted lines represent the standard deviation of the normalized data and the solid line is the PARC solution for a laminar free stream which has been similarly normalized. The conclusion to be drawn from this figure is that a good prediction of the heat transfer at a given surface distance from the stagnation point can be obtained by first using equation (11) to predict the stagnation heat transfer and then multiplying by the ratio of local to stagnation heat transfer from a solution for a laminar free stream.

SUMMARY OF CONCLUSIONS

Spanwise average stagnation region heat transfer measurements have been made on a model with a circular leading edge downstream of five turbulence generators. Four of the turbulence generators were square mesh, square bar, biplane grids with identical mesh spacing to bar width ratios and bar widths ranging from 0.16 to 1.27 cm. The fifth turbulence generator was an array of fine, parallel wires with the wires oriented normal to the axis of the cylindrical leading edge. Cylinder Reynolds numbers ranged from 42,000 to 193,000, turbulence intensities ranged from 1.1 to 15.9%, and the ratio of integral length scale to cylinder diameter ranged from 0.05 to 0.30. Conclusions are summarized as follows:

1. Low turbulence heat transfer results agree with both the Frossling solution and a numerical solution to within estimated experimental accuracy validating the experimental method.
2. Augmentation of stagnation region heat transfer by turbulence increases as integral length scale decreases.
3. No optimum length scale was found for the turbulence generating grids used in the present test ($\Lambda_x/d \geq 0.05$).
4. A correlation for stagnation heat transfer for the four square bar grids was developed which reduced data scatter to $\pm 4\%$.
5. The stagnation heat transfer data of other authors with similar turbulence generators was predicted to within $\pm 8\%$ by the correlation.
6. The correlation did not predict the heat transfer for the array of parallel wires indicating that augmentation must also be a function of isotropy of the turbulent flow field. This was also true for the data of other authors who generated anisotropic turbulence.
7. Frossling number downstream of stagnation normalized by the stagnation value can be represented by a universal curve for both laminar and turbulent flow.

REFERENCES

1. Frossling, N., "Evaporation, Heat Transfer, and Velocity Distribution in Two-Dimensional and Rotationally Symmetrical Laminar Boundary-Layer Flow," NACA TM-1432, 1958
2. Zimmerman, D. R., "Laser Anemometer Measurements at the Exit of a T63-C20 Combustor," NASA CR - 159623, 1979
3. Morkovin, M.V., "On the Question of Instabilities Upstream of Cylindrical Bodies," NASA CR-3231, Dec. 1979
4. Hanarp, L.R., Suden, B.A., "Structure of the Boundary Layers on a Circular Cylinder in the Presence of Free Stream Turbulence," *Letters in Heat and Mass Transfer*, Volume 9, 1982, pages 169-177
5. Van Fossen G.J., Simoneau, R.J., "A Study of the Relationship Between Free-Stream Turbulence and Stagnation Region Heat Transfer," *J. of Heat Transfer*, Volume 109, 1987, pages 10-15
6. Rigby, D.L., Van Fossen, G.J., "Increased Heat Transfer to a Cylindrical Leading Edge due to Spanwise Variations in the Free-stream Velocity," presented at the AIAA 22nd Fluid Dynamics, Plasma Dynamics & Lasers Conf., Honolulu, HA, June 24-26, 1991 AIAA-91-1739, also NASA TM 104464
7. Giedt, W. H., "Effect of Turbulence Level of Incident Air Stream on Local Heat Transfer From Cylinders," *J. of the Aeronautical Sciences*, Vol. 18, No. 11, 1951, pages 725-730

8. Seban, R. A., "The Influence of Free Stream Turbulence on the Local Heat Transfer From Cylinders," *Journal of Heat Transfer*, Vol. 82c, May 1960, pages 101-107
9. Zapp, G. M., "The Effect of Turbulence on Local Heat Transfer Coefficient Around a Cylinder Normal to an Air Stream," M.S. Thesis, Oregon State College, June 1950
10. Schnautz, John A., "Effect of Turbulence Intensity on Mass Transfer from Plates, Cylinders, and Spheres in Air Streams," PhD Thesis, Oregon State College, June 1958
11. Smith, M. C. and Kuethe, A. M., "Effects of Turbulence on Laminar Skin Friction and Heat Transfer," *The Physics of Fluids*, Vol. 9, No. 12, Dec., 1966, pages 2337-2344
12. Kestin, J., Wood, R. T., "The Influence of Turbulence on Mass Transfer From Cylinders." *Trans. of the ASME, J. of Heat Transfer*, Vol 93 C, 1971, pages 321-327
13. Mehendale, A. B., Han, J. C., Ou, S.; "Influence of High Mainstream Turbulence on Leading Edge Heat Transfer," *J. of Heat Transfer*, Vol. 113, 1991, pages 843-850
14. Lowery, G. W. and Vachon, R. I., "Effect of Turbulence on Heat Transfer From Heated Cylinders," *International J. of Heat and Mass Transfer*, V18 No. 11, 1975, pages 1229-1242
15. O'Brien, James E., Van Fossen, G. James, "The Influence of Jet-Grid Turbulence on Heat Transfer from the Stagnation Region of a Cylinder in Crossflow," presented at the ASME National Heat Transfer Conference, Denver, CO, Aug. 4-7, 1985, also NASA TM 87011
16. Yardi, N. R. and Sukhatme, S. P., "Effects of Turbulence Intensity and Integral Length Scale of a Turbulent Free Stream on Forced Convection Heat Transfer From a Circular Cylinder in Cross Flow," *Proc. of the 6th Int. Heat Transfer Conf.*, paper no. FC(b)-29, 1978, pages 347-352
17. Dyban, YE. P., Epic, E. YA., and Kozlova L. G., "Heat Transfer in the Vicinity of the Front Stagnation point of a Cylinder in Transverse Flow," *HEAT TRANSFER - Soviet Research*, Vol. 7, No.2, March-April, 1975, pages 70-73
18. Ames, Forrest E., "Heat Transfer with High Intensity, Large Scale Turbulence: The Flat Plate Turbulent Boundary Layer and the Cylindrical Stagnation Point," PhD Thesis, Stanford Univ., 1990
19. Hunt, J.C.R., "A Theory of Turbulent Flow Round Two-Dimensional Bluff Bodies," *J. of Fluid Mechanics*, Volume 61, Part 4, 1973, pages 625
20. Hunt, J.C.R., Graham, J.M.R., "Free-Stream Turbulence Near Plane Boundaries," *J. of Fluid Mechanics*, Volume 84, 1978, pages 209-
21. Van Fossen, G.J., Simoneau, R.J., Olsen, W.A., Jr., Shaw, R.J., "Heat Transfer Distributions Around Nominal Ice Accretion Shapes Formed on a Cylinder in the NASA Lewis Icing Research Tunnel," presented at the AIAA 22nd Aerospace Sciences Meeting, Jan. 9-12, 1984, Reno, NV, paper no. AIAA-84-0017; also NASA TM-83557

22. Miller, R.L., "ESCORT: A Data Acquisition and Display System to Support Research Testing," NASA TM-78909, 1978
23. Anon., *DISA Type 55M25 Linearizer Instruction Manual*, published by DISA Information Department, page 7, example 1.
24. Champagne, F.H., Sleicher, C.A., Wehrmann, O.H., "Turbulence Measurements with Inclined Hot Wires," *J. of Fluid Mechanics*, Volume 28, 1967, pages 153-182
25. Van Fossen, G.J., Simoneau, R.J., Ching, C.Y., "The Influence of Turbulence Parameters and Velocity Gradient on Stagnation Region Heat Transfer," NASA TP to be published.
26. Wiegand, R.A., "Grid Generated Turbulence with and without Rotation about the Streamwise Direction," PhD Thesis, Illinois Institute of Tech., Chicago, IL, 1978
27. Tan-Atichat, J., "Effects of Axisymmetric Contractions on Turbulence of Various Scales," PhD Thesis, Illinois Inst. of Tech., Chicago, IL, 1980
28. Rigby, D.L., Van Fossen G.J., "Increased Heat Transfer to Elliptical Leading Edges due to Spanwise Variations in the Freestream Momentum: Numerical and Experimental Results," presented at the AIAA/SAE/ASME/ASEE 28th Joint Propulsion Conference and Exhibit, July 6-8, 1992, Nashville, TN, AIAA paper no. AIAA 92-3070
29. Hillsenrath, J., Beckett, C.W., Benedict, W.S., Fano, L., and Hobe, H.J., "Tables of Thermal Properties of Gases," NBS Circular 564, Nov. 1955
30. Kline, S. J., McClintock, F. A., "*Describing UNCERTAINTIES in SINGLE-SAMPLE EXPERIMENTS*," *Mechanical Engineering*, Volume 75, Jan. 1953, pages 3-8
31. Baines, W. D., Peterson, E.G., "An Investigation of Flow Through Screens," *Trans. of the ASME*, Volume 72, July 1951, pages 468-480
32. Roach, P.E., "The generation of nearly isotropic turbulence by means of grids," *Int. J. of Heat and Fluid Flow*, Volume 8 No. 2, June, 1987, pages 82-92
33. Yeh, F. C., Hippensteele, S.A., Van Fossen, G.J., Poinsatte, P.E., Ameri, A., "High Reynolds Number and Turbulence Effects on Aerodynamics and Heat Transfer in a Turbine Cascade," presented at the AIAA/SAE/ASME/ASEE 29th Joint Propulsion Conference and Exhibit, Monterey, CA, June 28-30, 1993, paper no. AIAA-93-2252

Table I. Turbulence grid dimensions.

GRID NO.	b, cm (in)	M/b	% OPEN AREA
G1	1.270(.500)	4.5	60.5
G2	0.635(.250)	4.5	60.5
G3	0.318(.125)	4.5	60.5
G4	0.159(.063)	4.5	60.5
G5*	0.051(.020)	12.5	92.0

*Grid G5 - array of parallel wires

Table II. Power law curve fits of turbulence intensity and integral length scale data.

$$Tu = a \left(\frac{x}{b} \right)^m \qquad \frac{\Lambda_x}{b} = I \left(\frac{x}{b} \right)^p$$

Grid	Velocity symbol	Re _b	a	m	I	p
G1	R1	38650	206.1	-0.875	0.240	0.500
G1	R2	18000	206.1	-0.875	0.240	0.500
G1	R3	7934	206.1	-0.875	0.240	0.500
G2	R1	17190	146.3	-0.780	0.272	0.500
G2	R2	9514	135.3	-0.758	0.272	0.500
G2	R3	4452	138.9	-0.778	0.272	0.500
G3	R1	8935	132.2	-0.765	0.264	0.500
G3	R2	4780	156.3	-0.824	0.264	0.500
G3	R3	2470	149.4	-0.830	0.264	0.500
G4	R1	4571	80.15	-0.665	0.303	0.500
G4	R2	2297	89.46	-0.693	0.303	0.500
G4	R3	1174	75.05	-0.677	0.303	0.500
G5	R1	1634	23.68	-0.470	4.658	0.116
G5	R2	792	23.38	-0.453	3.255	0.199
G5	R3	340	52.73	-0.568	10.011	0.051

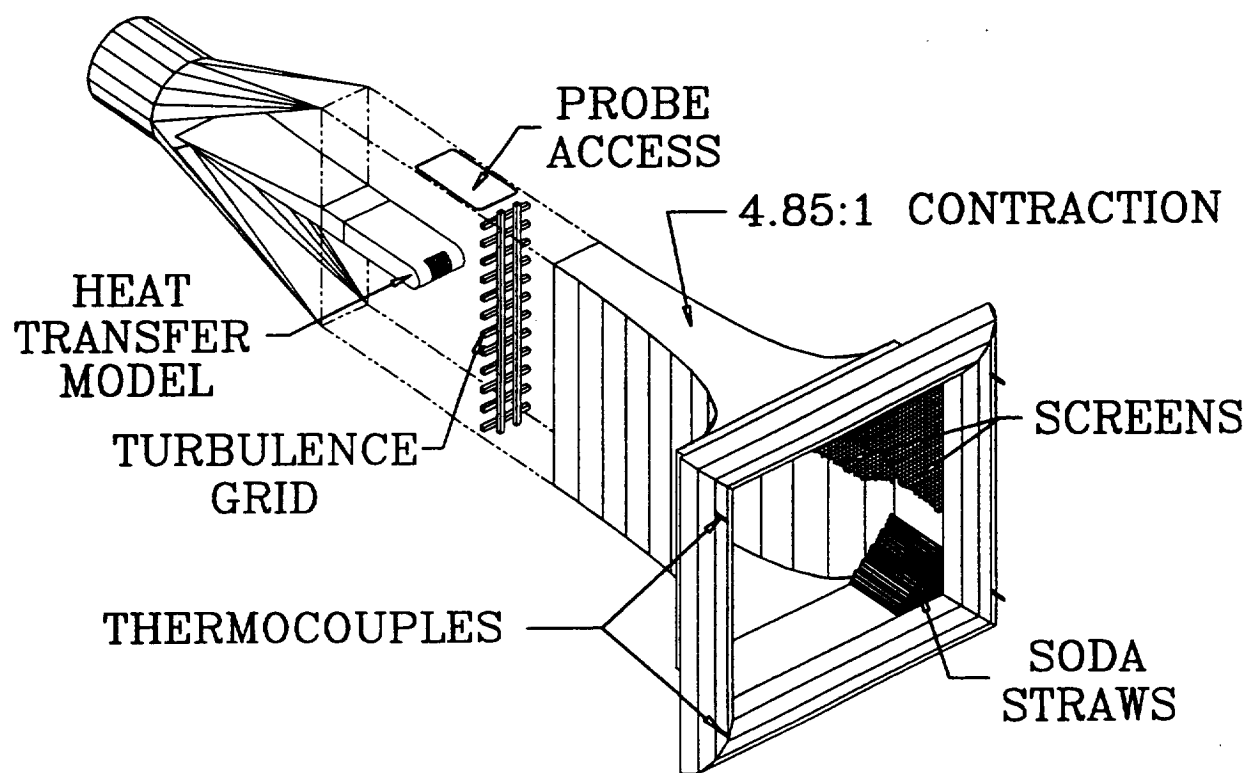


Figure 1. Wind tunnel.

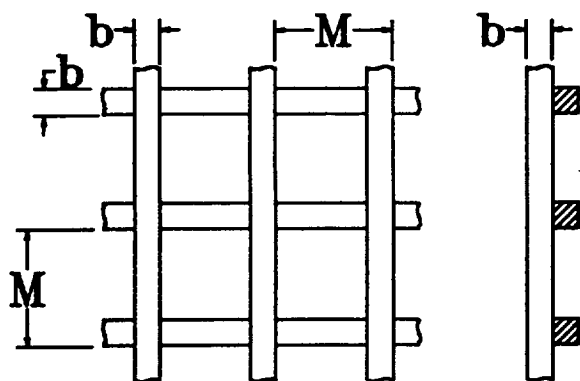


Figure 2. Biplane grid configuration.

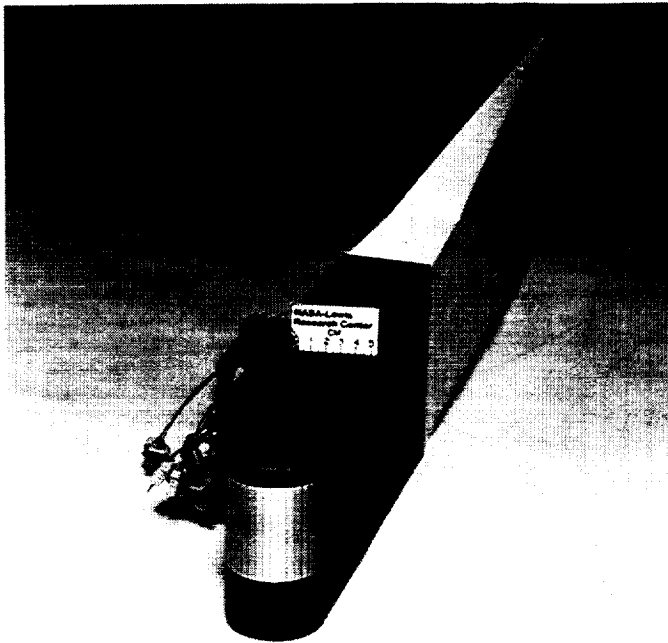


Figure 3. Heat transfer model.

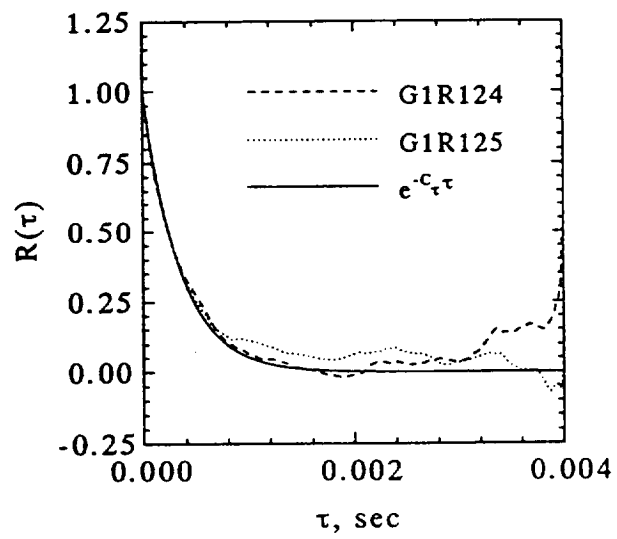


Figure 4. Typical autocorrelations for successive readings.

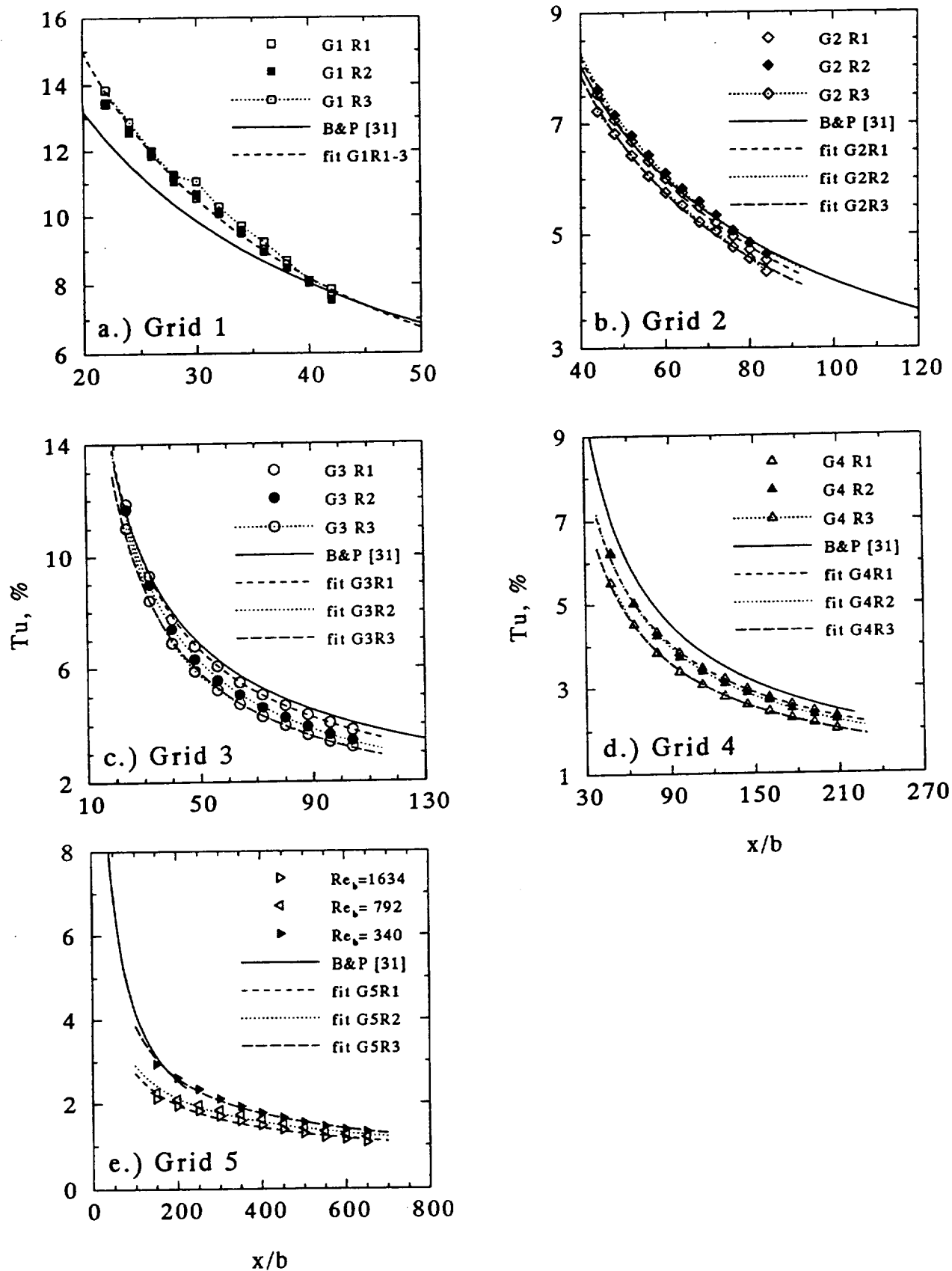


Figure 5. Turbulence intensity data and curve fit compared to data of [31].

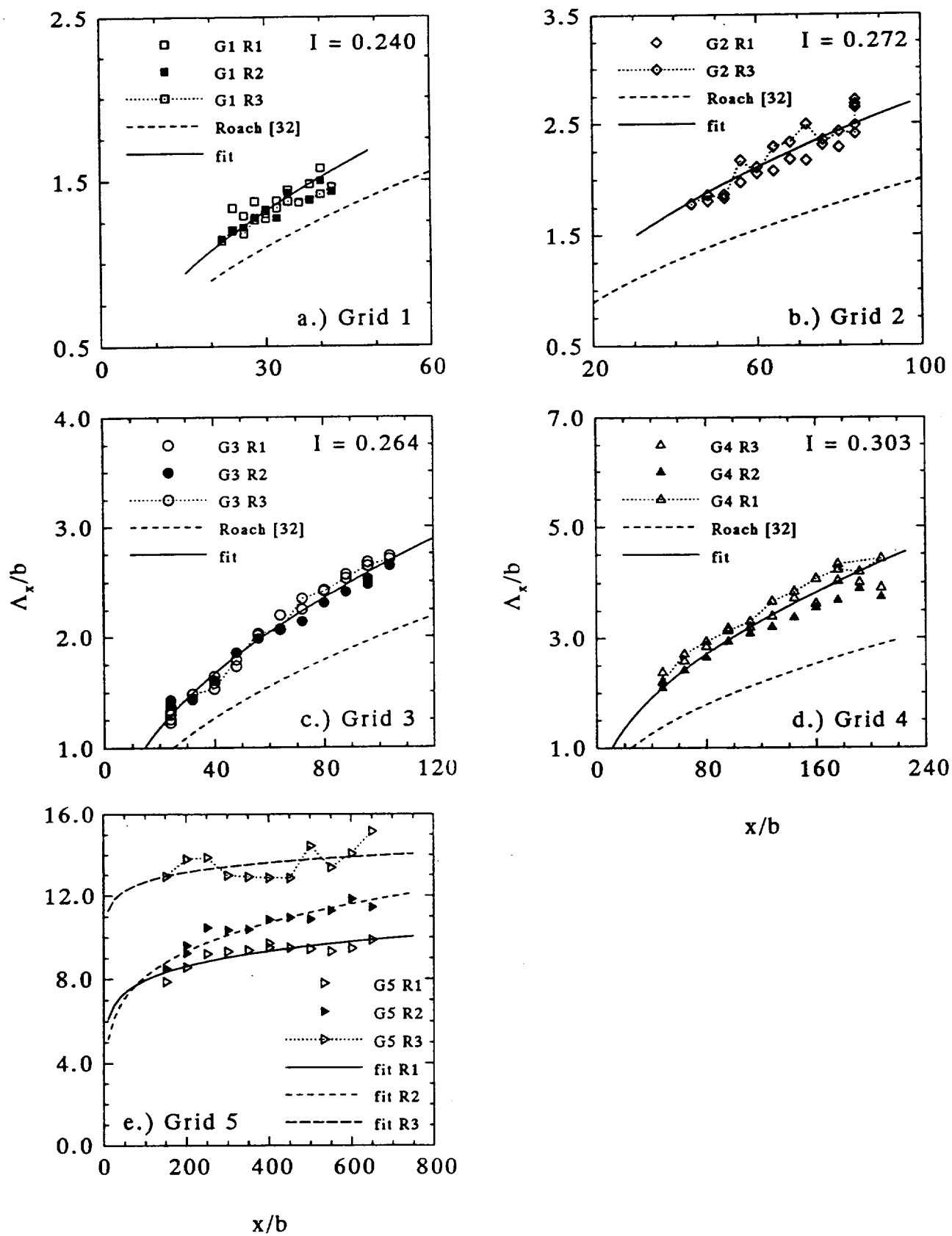


Figure 6. Length scale versus distance from the grid compared to curve fit and theory of [32].

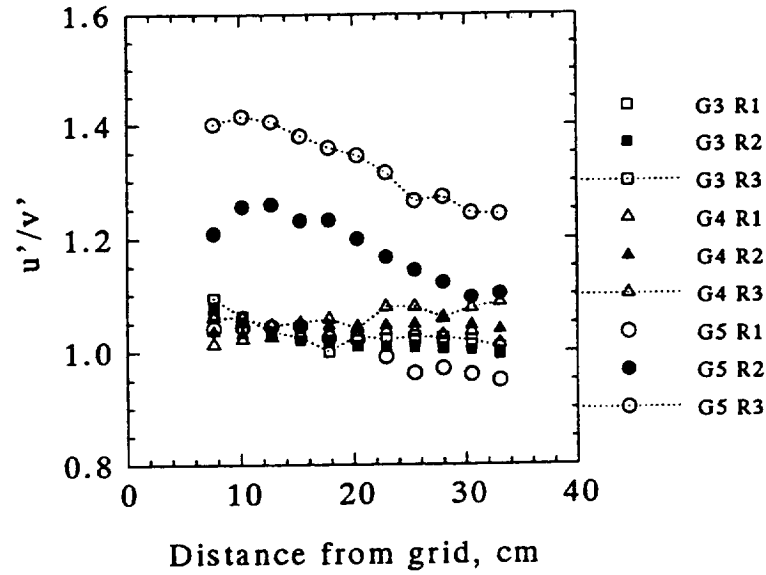


Figure 7. Isotropy of turbulence from grids 3, 4, and 5.

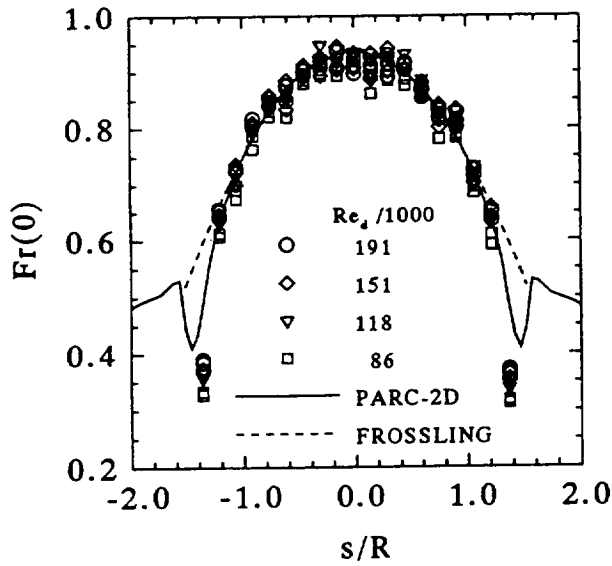


Figure 8. Frossling number distribution compared to PARC and Frossling solutions.

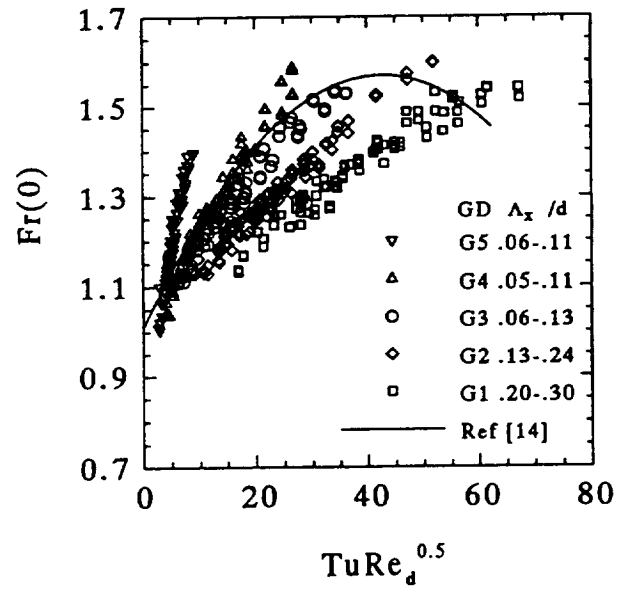


Figure 9. Stagnation point Frossling number vs $TuRe_d^{1/2}$ showing the effect of length scale.

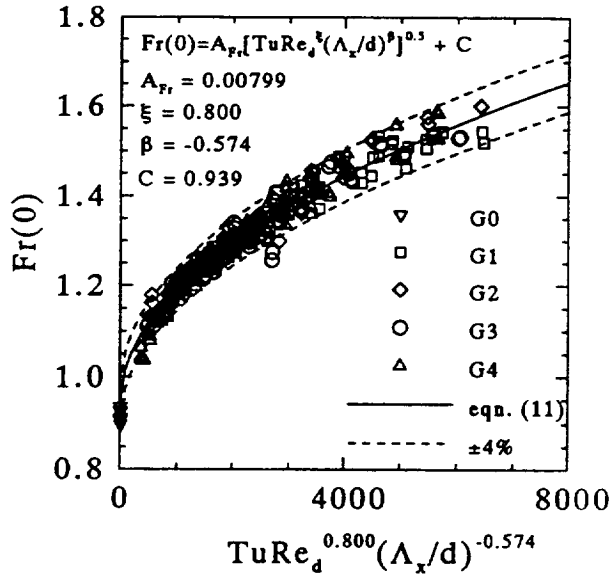


Figure 10. Stagnation point Frossling number for grids G1-G4 versus correlation parameter.

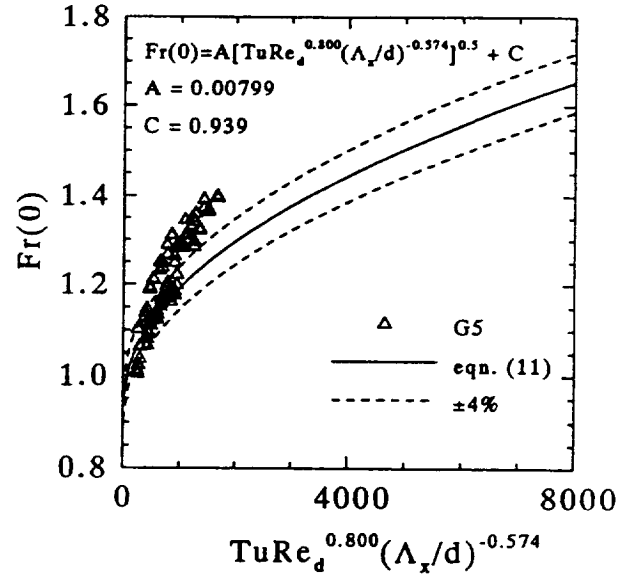


Figure 11. Comparison of stagnation Frossling number with grid G5 data (parallel wires).

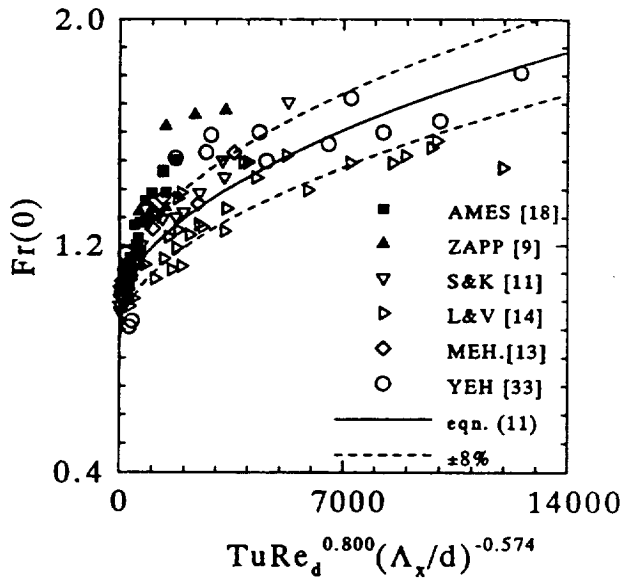


Figure 12. Stagnation Frossling number data of other authors compared to correlation.

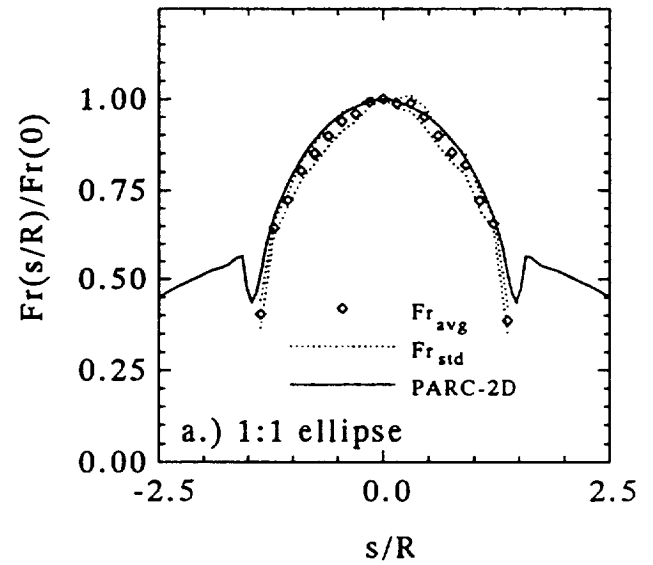


Figure 13. Distribution of averaged, normalized Frossling number downstream of stagnation point.

Keywords: Heat transfer, Stagnation flow, Turbulence, Length scale, Leading edge

REPORT DOCUMENTATION PAGE			Form Approved OMB No. 0704-0188	
Public reporting burden for this collection of information is estimated to average 1 hour per response, including the time for reviewing instructions, searching existing data sources, gathering and maintaining the data needed, and completing and reviewing the collection of information. Send comments regarding this burden estimate or any other aspect of this collection of information, including suggestions for reducing this burden, to Washington Headquarters Services, Directorate for Information Operations and Reports, 1215 Jefferson Davis Highway, Suite 1204, Arlington, VA 22202-4302, and to the Office of Management and Budget, Paperwork Reduction Project (0704-0188), Washington, DC 20503.				
1. AGENCY USE ONLY (Leave blank)	2. REPORT DATE February 1994	3. REPORT TYPE AND DATES COVERED Technical Memorandum		
4. TITLE AND SUBTITLE Measurements of the Influence of Integral Length Scale on Stagnation Region Heat Transfer		5. FUNDING NUMBERS WU-505-62-52		
6. AUTHOR(S) G. James Van Fossen and Chan Y. Ching				
7. PERFORMING ORGANIZATION NAME(S) AND ADDRESS(ES) National Aeronautics and Space Administration Lewis Research Center Cleveland, Ohio 44135-3191		8. PERFORMING ORGANIZATION REPORT NUMBER E-8532		
9. SPONSORING/MONITORING AGENCY NAME(S) AND ADDRESS(ES) National Aeronautics and Space Administration Washington, D.C. 20546-0001		10. SPONSORING/MONITORING AGENCY REPORT NUMBER NASA TM-106503		
11. SUPPLEMENTARY NOTES Prepared for the Fifth Symposium on Transport Phenomena and Dynamics of Rotating Machinery sponsored by the Pacific Center of Thermal Fluids Engineers, Kaanapali, Hawaii, May 8-11, 1994. G. James Van Fossen, NASA Lewis Research Center; Chan Y. Ching, Syracuse University, Syracuse, New York 13210. Responsible person, G. James Van Fossen, organization code 2630, (216) 433-5892.				
12a. DISTRIBUTION/AVAILABILITY STATEMENT Unclassified - Unlimited Subject Category 34		12b. DISTRIBUTION CODE		
13. ABSTRACT (Maximum 200 words) The purpose of the present work was twofold: first, to determine if a length scale existed that would cause the greatest augmentation in stagnation region heat transfer for a given turbulence intensity and second, to develop a prediction tool for stagnation heat transfer in the presence of free stream turbulence. Toward this end, a model with a circular leading edge was fabricated with heat transfer gages in the stagnation region. The model was qualified in a low turbulence wind tunnel by comparing measurements with Frossling's solution for stagnation region heat transfer in a laminar free stream. Five turbulence generating grids were fabricated; four were square mesh, biplane grids made from square bars. Each had identical mesh to bar width ratio but different bar widths. The fifth grid was an array of fine parallel wires that were perpendicular to the axis of the cylindrical leading edge. Turbulence intensity and integral length scale were measured as a function of distance from the grids. Stagnation region heat transfer was measured at various distances downstream of each grid. Data were taken at cylinder Reynolds numbers ranging from 42,000 to 193,000. Turbulence intensities were in the range 1.1 to 15.9 percent while the ratio of integral length scale to cylinder diameter ranged from 0.05 to 0.30. Stagnation region heat transfer augmentation increased with decreasing length scale. An optimum scale was not found. A correlation was developed that fit heat transfer data for the square bar grids to within $\pm 4\%$. The data from the array of wires were not predicted by the correlation; augmentation was higher for this case indicating that the degree of isotropy in the turbulent flow field has a large effect on stagnation heat transfer. The data of other researchers are also compared with the correlation.				
14. SUBJECT TERMS Heat transfer; Turbulence; Stagnation; Length scale		15. NUMBER OF PAGES 22		
		16. PRICE CODE A03		
17. SECURITY CLASSIFICATION OF REPORT Unclassified	18. SECURITY CLASSIFICATION OF THIS PAGE Unclassified	19. SECURITY CLASSIFICATION OF ABSTRACT Unclassified	20. LIMITATION OF ABSTRACT	